Applied Catalysis B: Environmental 140–141 (2013) 546–551

Contents lists available at SciVerse ScienceDirect

Applied Catalysis B: Environmental

journal homepage: www.elsevier.com/locate/apcatb

Photocatalytically enhanced Cr(VI) removal by mixed oxides derived from MeAl (Me:Mg and/or Zn) layered double hydroxides

Claudia Alanis[a], Reyna Natividad[a,*], Carlos Barrera-Diaz[a], Verónica Martínez-Miranda[b], Julia Prince[c], Jaime S. Valente[d,**]

[a] Centro Conjunto de Investigación en Química Sustentable, UAEMéx-UNAM, km 14.5 carretera Toluca-Atlacomulco, San Cayetano, Piedras Blancas, Toluca, Estado de México, Mexico
[b] Centro Interamericano de Recursos del Agua, Facultad de Ingeniería, Universidad Autónoma del Estado de México, Centro de Coatepec, Toluca, Estado de México, Mexico
[c] Universidad Autónoma Metropolitana-A, Química de Materiales, Avenida San Pablo No. 180, 02200 México, DF, Mexico
[d] Instituto Mexicano del Petróleo, Eje Central # 152, México, DF 07730, Mexico

ARTICLE INFO

Article history:
Received 31 October 2012
Received in revised form 16 April 2013
Accepted 26 April 2013
Available online 4 May 2013

Keywords:
Adsorption
Photoreduction
Chromium (VI) reduction
Hydrotalcites
Photocatalysis

ABSTRACT

This work aims to present a study of the adsorption and photocatalytic reduction of Cr(VI) by ZnAl, MgZnAl and MgAl mixed oxides derived from layered double hydroxides (LDHs). The effect of variables like Zn content and pH (3 and 6.5) on Cr(VI) removal efficiency is presented. The catalysts were characterized by X-ray diffraction (XRD) and infrared spectroscopy (FTIR). The reaction progress was verified by UV/vis spectrophotometry with a colorimetric method. A maximum of 99.5% Cr(VI) was photocatalytically removed and this process was approximately two times faster than adsorption. In addition, it was found that the use of these materials does not imply the addition of further chemicals to regulate pH since the free basic pH of the catalyst-contaminant suspension positively affects both adsorption and photo-reduction kinetics.

© 2013 Elsevier B.V. All rights reserved.

1. Introduction

The most common chromium oxidation states in nature are Cr(III) and Cr(VI). However, hexavalent chromium is carcinogenic and toxic; whereas Cr(III) is 1000 times less toxic than Cr(VI) [1]. This toxic metal is typically discharged in effluents of industries such as the textile, leather tanning, paint, pigment manufacturing, photography, chrome plating, wood preservation and fertilizers. The concentration in water of such a metal should not exceed 10 mg L^{-1} for the protection of aquatic species and therefore the permissible discharge limit of Cr(VI) for such industrial water streams is between 0.1 and 0.5 mg L^{-1}. Thus, the removal of hexavalent chromium or its reduction to trivalent chromium is compulsory in order to protect the public health and environment [2–7]. Cr(VI) elimination from wastewater includes processes such as chemical reduction and precipitation, coagulation, membrane separation, oxidation-reduction, ion exchange, electrochemical and adsorption [8]. Although these methods are effective they have some disadvantages such as sludge generation, exhausted materials disposal and high operational costs that restrict their use [4,5]. In this context, photocatalysis has attracted the attention of the scientific community since it is a rapid and efficient method for the destruction of environmental pollutants. In photocatalytic processes a semiconductor is illuminated with light of energy greater than the semiconductor band gap, thus producing electron–hole pairs (e-/h+) in the conduction and the valence bands of the semiconductor, respectively. These charge carriers, which migrate to the semiconductor surface, are capable of reducing or oxidizing species in solution having suitable redox potentials. The reducing capacity of the semiconductor photocatalyst which uses the electrons generated on the semiconductor surface is, however, scarcely assessed compared to its oxidizing ability [9]. Actually, only the use of the catalysts TiO_2 and ZnO has been reported [9–13]. The use of these photo-catalysts, however, usually requires a relatively large amount of catalyst and the addition of chemicals to keep an acid pH in order to achieve 90–94% Cr(VI) reduction.

These facts encourage the search of other catalytic materials that could be employed under lower concentrations and at pH that does not require the addition of chemicals. In this context, the calcined hydrotalcite like compounds or layered double hydroxides

* Corresponding author. Tel.: +52 722 2766610x7723.
** Corresponding author. Tel.: +52 55 9175 8444.
E-mail addresses: reynanr@gmail.com (R. Natividad), jsanchez@imp.mx (J.S. Valente).

0926-3373/$ – see front matter © 2013 Elsevier B.V. All rights reserved.
http://dx.doi.org/10.1016/j.apcatb.2013.04.053

(LDHs) emerge as an attractive alternative since they have already been proven as efficient photocatalysts to perform the oxidation of organic compounds such as phenols and their halogenates [14,15]. In this work, MgZnAl and ZnAl layered double hydroxides are investigated for the first time as precursors of photocatalysts for a reduction process.

Layered double hydroxides (LDHs) are from the family of anionic clays. Their structure is based on brucite-like layers, wherein partial isomorphic substitution of divalent cations for trivalent cations produces layered materials consisting of positively charged host layers. This charge is balanced by anionic species located in the interlayer region along with hydration molecules. The basic structure can be represented by the general formula: $[M_{(1-x)}^{II}M_x^{III}(OH)_2]\,A_{x/n}^{n-}\,mH_2O$, where M^{II} includes: Mg^{2+}, Co^{2+}, Cu^{2+}, Ni^{2+}, Zn^{2+}, etc.; M^{III} may be Al^{3+}, Cr^{3+}, In^{3+}, Mn^{3+}, Ga^{3+}, Fe^{3+}, and A^{n-} might be any organic and/or inorganic anions. Many ternary LDHs involving mixtures of different M^{II} and/or M^{III} may also be prepared [16–18]. LDH's have been studied as catalysts or catalyst precursors to a great extent for the past few decades [17–19]. Their most interesting properties are high surface area, basic sites, homogeneous interdispersion of the elements, formation upon calcination of thermally stable mixed metal oxides M^{2+} (M^{3+}) O, synergetic effects between the elements and the memory effect, which allows regeneration of the original structure under mild conditions [17,20–22]. After calcination, the product of LDHs are mixed oxides; solids with basic properties [23,24], which have been successfully employed in many organic reactions catalyzed by bases. Moreover, LDHs have been employed in a wide range of technological applications, such as hybrid composites, antacid agents, flame retardants and PVC additives. In addition, several research groups worldwide have attempted to introduce biological species and organic compounds between layers [25,26].

Photocatalytic applications of LDHs are an interesting emerging field. Several semiconducting mixed oxides derived from LDHs have been studied for the photocatalytic degradation of contaminants, such as ZnAl [27–29], ZnAlFe [30] and MgZnAl [22] LDHs. Also, because of their anion-exchange capacity, LDHs have been tested as adsorbents to remove anionic pollutants from water [22]. Therefore, this paper focuses on studying the photocatalytic and adsorption capabilities of mixed oxides derived from ZnAl, MgZnAl and MgAl LDHs on the removal of hexavalent chromium from aqueous solutions.

2. Experimental

2.1. Synthesis

ZnAl, MgAl and MgZnAl LDHs containing 5 and 10 weight percentage of Zn were synthesized by the co-precipitation method at constant pH of 9 as reported in literature [15]. The resulting solids were calcined at 500 °C during 4 h (heating ramp of 1 °C/min) under dry air flow prior to adsorption and heterogeneous photocatalytic tests. Solids were named according to their chemical composition, i.e. ZnAl, MgAl or MgZnAl-*x*, where *x* stands for the nominal weight % of zinc.

2.2. Adsorption tests

Adsorption tests of Cr(VI) onto TiO_2 (Degussa P25) and calcined ZnAl, MgZnAl-5, MgZnAl-10 and MgAl LDHs were carried out in a glass reactor (0.236 m long and 0.03 m of diameter) under continuous stirring (800 rpm). The Cr(VI) solution was prepared by diluting in deionized water a proper amount of K_2CrO_7 in order to obtained an initial concentration of Cr(VI) ($C_{o,Cr(VI)}$) of 0.046 mmol L^{-1}. The total suspension volume was 100 mL. The test was performed using 1 g L^{-1} of calcined LDH at different pH values (3 and 6.5). The pH 3 was adjusted by using 0.1 M H_2SO_4 solution while pH 6.5 is the one attained when preparing the solution. Thus working at initial pH of 6.5 does not imply further addition of chemicals. The reactor temperature was maintained constant at 25 ± 1 °C. Aliquots samples (1.0 mL) were withdrawn from the system every 5 min during 70 min. These samples were centrifuged to separate the adsorbent material and the supernatant. The former was taken to XRD while the latter was analyzed by UV–vis spectroscopy.

2.3. Photocatalytic tests

The photocatalytic reduction tests of Cr(VI) to Cr(III) were carried out as in adsorption. In this case, however, a UV lamp was employed. This lamp was inserted at the center of the reactor as the source of UV radiation (254 nm at 4500 μW cm^{-2}). The reactor temperature was maintained constant at 25 ± 1 °C. At specific time ranges (5, 10, 15, 20, 25, 30, 35 to 70 min) the test solutions were centrifuged to separate the adsorbent material and the supernatant. In this case the solid was characterized prior and after photocatalytic tests by XRD and IR.

2.4. Cr(VI) concentration quantification in aqueous solution

The methodology for determining hexavalent chromium concentration in aqueous solution was the colorimetric method based on the NMX-AA-044-SCFI-2001 Mexican standard. In concordance with this method, samples were analyzed by UV at 543 nm after complexation with 1, 5-diphenilcarbazide. The solution was analyzed for aqueous metal concentration using the standard method of Cr(VI) detection using UV–vis spectrophotometry (PerkinElmer lambda 25). A calibration curve was constructed from 0 to 0.009 mmol L^{-1} of Cr(VI) concentration, obtaining a determination coefficient of $r^2 = 0.9983$ and a slope $\varepsilon b = 0.5162$ of Beer's Law. All experiments were performed three times to verify the reliability of results.

2.5. Fourier transform infrared spectroscopy (FTIR)

The DRIFT spectra of MgAl, MgZnAl-*x* and ZnAl LDHs after photocatalytic reduction were recorded with a Bruker Equinox 55 spectrophotometer equipped with a Harrick diffuse reflection attachment (HDRPBR-3), at a resolution of 4 cm^{-1} and averaging over 300 scans, in the range 4000–400 cm^{-1}. Solids were placed in the sampler cup and the spectra were recorded at room temperature.

2.6. X-ray diffraction

ZnAl, MgZnAl-*x* and MgAl LDHs were analyzed by XRD in a Bruker D8 Advanced diffractometer with Cu Kα radiation and a Lynxeye™ detector. The specific analysis conditions were: 30 kV, 25 mA, diffraction intensity was measured between 5 and 80°, 2θ step of 0.02°, and a counting time of 31.8 s. The analysis was conducted prior and after adsorption and photocatalytic tests.

2.7. Textural analysis

The texture of the calcined samples (at 500 °C for 6 h in air) was analyzed by N_2 adsorption–desorption at −196 °C on a Quantachrome Autosorb-3B apparatus. Prior to the analysis, the calcined samples were outgassed in a vacuum (10^{-5} Torr) at 400 °C for 12 h. The surface areas were calculated by the Brunauer–Emmett–Teller (BET) method, and the pore size distribution and total pore volume

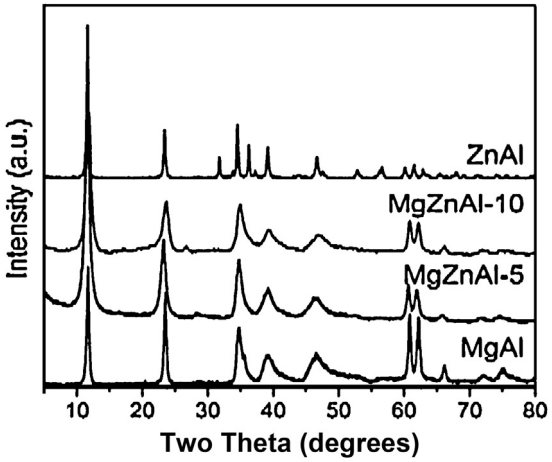

Fig. 1. X-ray diffractograms for the as-synthesized LDHs samples.

were determined by the Brunauer–Joyner–Hallenda (BJH) method applied to the desorption branch.

3. Results and discussion

3.1. Characterization of solids prior to adsorption and photocatalytic tests

3.1.1. X-ray diffraction

Fig. 1 depicts the XRD patterns for the LDH precursors MgAl, MgZnAl-5, MgZnAl-10 and ZnAl. All samples show pure LDH structure, with sharp peaks indicating a highly crystalline structure [22]. Solids MgAl, MgZnAl-5 and MgZnAl-10 present a 3R polytype, which is commonly found in most synthetic LDHs; meanwhile, sample ZnAl crystallized in a 2H polytype, which is the most stable form for ZnAl LDHs.

3.1.2. Chemical and textural analyses

Samples were analyzed by ICP-AES to determine their chemical composition. The results are summarized in Table 1, where it can be seen that the zinc content of MgZnAl-5 and MgZnAl-10 samples are close to nominal values, within experimental error. Furthermore, the divalent to trivalent metal cation ratio is close to the nominal value of 3, ranging from 2.57 for ZnAl to 3.30 for MgZnAl-10 (Table 1). Typically, during LDH synthesis, localized pH variations result in the incomplete precipitation of metal cations, which are washed out at a latter step. Therefore, the obtained chemical compositions usually vary slightly from nominal values. Furthermore, sample ZnAl exhibits the highest Zn content (*ca.* 44%).

Calcined solids were further analyzed by N_2 physisorption in order to determine their textural properties. The obtained isotherms were of type IV according to the IUPAC classification [31] (data not shown), which correspond to mesoporous solids. Hysteresis loops were of type H3, ascribed to slit-shaped pores with non-uniform size and shape, which are created by the collapse of LDH sheets upon calcination. Another consequence of the calcination process is the loss of weight (approximately 40%) due to the elimination of water and interlayer nitrate ions. According to the determined pore diameter the calcined LDHs can be classified as mesoporous solids. The textural properties of all solids are listed in Table 1, where it may be observed that the highest surface area was obtained by the MgAl sample, while the lowest value corresponds to ZnAl. Meanwhile, the largest pore volume was 1.05 $cm^3\ g^{-1}$ for MgZnAl-5 sample, while the smallest pore volume again corresponds to ZnAl.

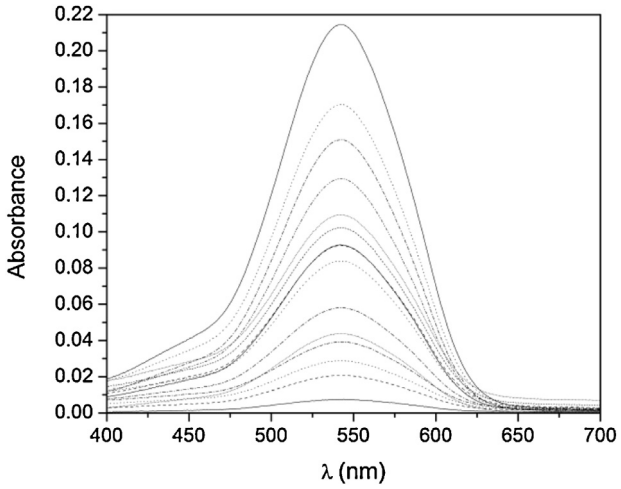

Fig. 2. UV–vis spectra of Cr(VI) solution for various times during the adsorption process using MgZnAl-5. $[Cr(VI)]_o = 4.6 \times 10^{-5}$ M $pH_o = 6.5$.

The band gap energy of the calcined solids was determined from the DR-UV–vis absorbance spectra (data not shown). It was observed that increasing zinc content brings about a decrease in band gap energy, from 5.45 in MgAl to 3.30 eV in ZnAl. Band gap energy values for all photocatalysts are presented in Table 1. TiO_2 related information is also included in Table 1 for reference purposes and this was obtained from literature [23].

3.2. Adsorption tests of Cr(VI) by calcined LDH's

3.2.1. Effect of Zn content

LDHs' affinity for CrO_4^{2-} has been previously reported [8,32–37]. In this work, however, the effect of Zn content on adsorption rate removal was studied. Fig. 2 shows typical UV–vis spectra when Cr(VI) adsorption process is carried out upon calcined MgZnAl-5. These spectra are characteristic of the obtained results by this technique with the other materials either by adsorption or photocatalysis.

The effect of Zn content on Cr(VI) fractional composition evolution with time by adsorption is presented in Fig. 3. In this figure the removal of anions containing Cr(VI) from solution by the all tested calcined LDH compounds is evident and can be ascribed to adsorption on external surface and reconstruction of calcined material. The latter is known as memory effect [17,38].

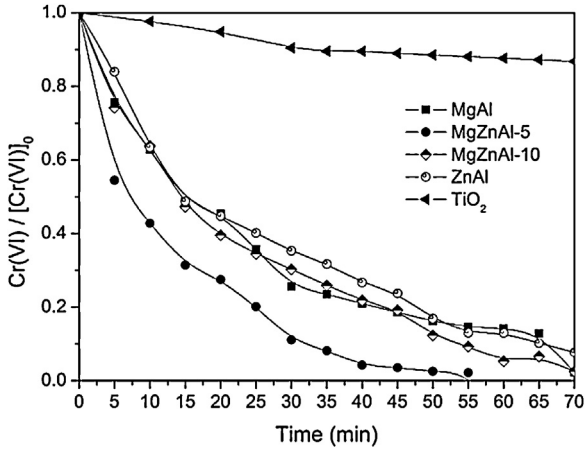

Fig. 3. Effect of Zn content on Cr(VI) removal from solution by adsorption. Experimental conditions: $pH_o = 6.5$, [sorbent]= 1 g L^{-1}, $[Cr(VI)]_o = 4.6 \times 10^{-5}$ M.

Table 1
Chemical composition, textural and semiconducting properties of tested materials.

Sample	Chemical formula	M^{II}/M^{III}	Zinc (wt%)	Pore Volume ($cm^3\,g^{-1}$)	S_{BET}(wt%) ($m^2\,g^{-1}$)	Pore Diameter (nm)	Band gap energy (eV)
MgAl	$[Mg_{0.745}\,Al_{0.255}(OH)_2](CO_3^{2-})_{0.13}H_2O$	2.93	–	0.62	276	18	5.45
MgZnAl-5	$[Mg_{0.65}Zn_{0.08}Al_{0.27}(OH)_2](CO_3^{2-})_{0.13}\cdot H_2O$	2.74	4.42	1.05	255	18	5.43
MgZnAl-10	$[Mg_{0.64}Zn_{0.13}Al_{0.23}(OH)_2](CO_3^{2-})_{0.12}\cdot H_2O$	3.30	9.25	0.84	182	18	4.47
ZnAl	$[Zn_{0.72}Al_{0.28}(OH)_2](CO_3^{2-})_{0.25}\cdot H_2O$	2.57	43.58	0.224	96.4	25	3.30
Degussa P-25	TiO_2	–	–	0.16	51	16	3.20

Mixed metal oxide is produced during the calcination process according to reaction (1) [34],

$$[M_{1-x}Al_x(OH)_2](NO_3)_{x/2} \rightarrow M_{1-x}Al_xO_{1+x/2} + \frac{x}{2}NO_2 + H_2O \quad (1)$$

The reconstruction of the hydrotalcite like structure is expected to occur by rehydration and incorporation of anions by reaction (2) [34],

$$M_{1-x}Al_xO_{1+x/2} + \left(\frac{x}{n}\right)A^{n-} + \left(1+\left(\frac{x}{2}\right)\right)H_2O \rightarrow [M_{1-x}Al_x(OH)_2](A^{n-})_{x/n} + xOH^- \quad (2)$$

In concordance with reaction (2), all tested materials should exhibit the ability of adsorbing Cr(VI) anions but at different rates. This adsorption rate was found to be a function of Zn content and may be related to the characteristic textural properties of each material, mainly pore volume which is observed to decrease in the same order than adsorption rate decreases, i.e. MgZnAl-5 > MgZnAl-10 > MgAl > ZnAl. The additional and combined effect of surface area and pore diameter cannot be disregarded though. In addition, an adsorption test was carried out with TiO_2 (Degussa P25) since this was also used as photocatalyst and the results are included as well in Fig. 3. It is not surprising that the adsorption with this oxide was not higher than 10%. TiO_2 has been proved [11] to be an efficient Cr(VI) sorbent at very low pH (~3) and it has been reported to be able to remove by adsorption up to 2.34 mg g^{-1} [39]. Such adsorption occurs by converting the ion of bichromate ($HCrO_4^-$) to the neutral chromate acid (H_2CrO_4) molecules under very acidic conditions and thus TiO_2 adsorption capacities have been reported to decrease when increasing pH [39,40]. At this point is worth mentioning that in the present study pH was not adjusted and all experiments presented here were carried out at the initial pH solution (6.5).

Nevertheless, since TiO_2 had been reported to be efficient at acidic pH a study of the effect of pH (3 and 6.5) was conducted and it was found that the most convenient pH was 6.5 for the calcined hydrotalcite like compounds. At acidic pH (1–4), the speciation diagram [11,41] of Cr(VI) indicates the presence of mainly three species (H_2CrO_4, $Cr_2O_7^{2-}$ and $HCrO_4^-$) while at basic pH (>8), the predominant anions are only two (CrO_4^{2-} and $HCrO_4^-$). That means that from the species of Cr(VI) formed at acidic pH, only two-thirds can be chemisorbed on sites present in the mixed oxide derived from LDHs. At this point it should be emphasized that the pH was modified adding H_2SO_4 and accordingly sulfate anions (SO_4^{2-}) are generated in solution, where they are expected to compete with Cr(VI) anions to fill the interlaminar space. It is not surprising that being divalent anions, SO_4^{2-} and CrO_4^{2-}, are adsorbed preferentially instead of the $HCrO_4^-$ [42] and thus excluding other species from the surface. By contrast, at alkaline pH the formed species only compete with each other and not with others, like may be occurring at acidic pH. It is worth clarifying that the effect of pH was studied from acidic values as an attempt to contrast our results with those reported elsewhere [32] where has been pointed out that the most effective pH range to conduct adsorption of Cr(VI) onto aluminum magnesium mixed oxides was 2.5–5.0. [32]. Also,

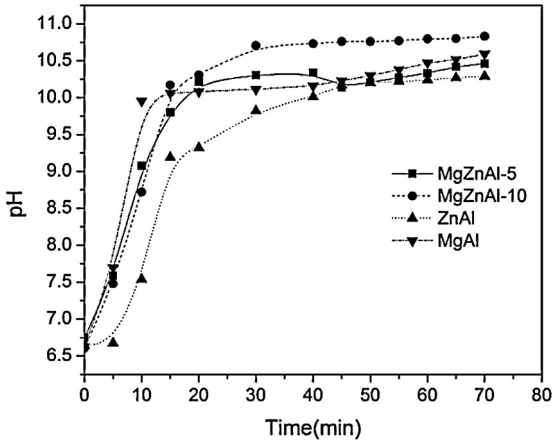

Fig. 4. Representative pH as function of time, during adsorption process $[Cr(VI)]_o = 4.6 \times 10^{-5}$ M and 1 g L^{-1} of MgAl, MgZnAl-5, MgZnAl-10 and ZnAl.

it has been reported [42] that a low pH favors Cr(VI) sorption from tannery wastewater onto hydrotalcites since competition does not exist and the retention of hydrotalcites structure is higher.

The initial pH at all experiments was 6.5 ± 0.5, however, an increase during the adsorption process was observed (Fig. 4). This increase could be attributable to the surface rehydroxilation [43] by water dissociation and can be correlated then with surface basicity, which can be tailored by the nature of the cations, compensating anions and the calcination temperature [24]. Also, as acidic anions are progressively adsorbed to the LDH surface and absorbed into the interlayer region, the pH is expected to increase.

Fig. 5 presents the XRD patterns of the different employed calcined LDH compounds after the adsorption process. These XRD patterns are also evidence of the reconstruction process since all solids tend to recover the original layered structure, and the only

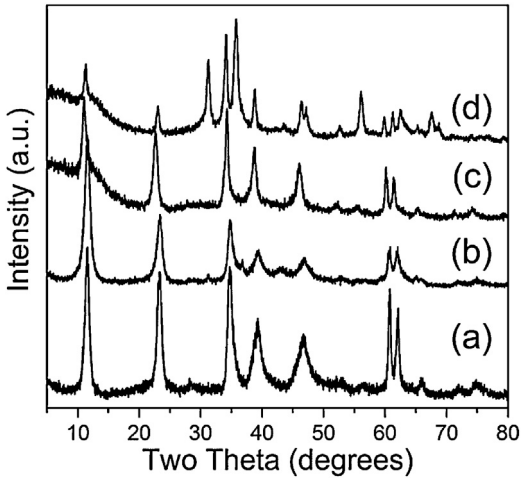

Fig. 5. XRD patterns for calcined LDHs, (a)MgAl, (b)MgZnAl-5, (c)MgZnAl-10 and (d) ZnAl after adsorption of CrO_4^{2-} for 70 min.

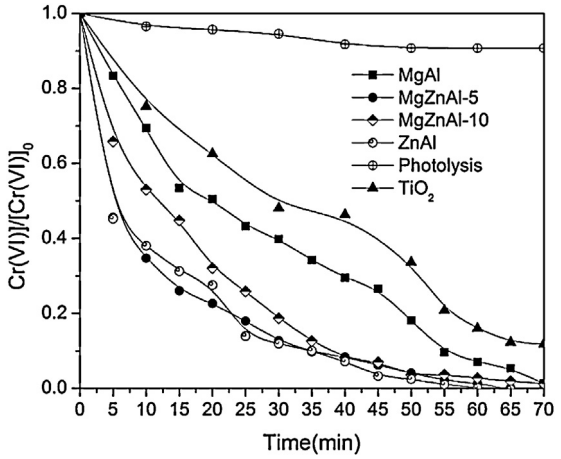

Fig. 6. Effect of Zn content on photocatalyzed Cr(VI) removal. $[Cr(VI)]_o = 4.6 \times 10^{-5}$ M, $V_{reaction} = 0.1$ L, $pH_o = 6.5$, $W_{cat} = 1$ g L^{-1}.

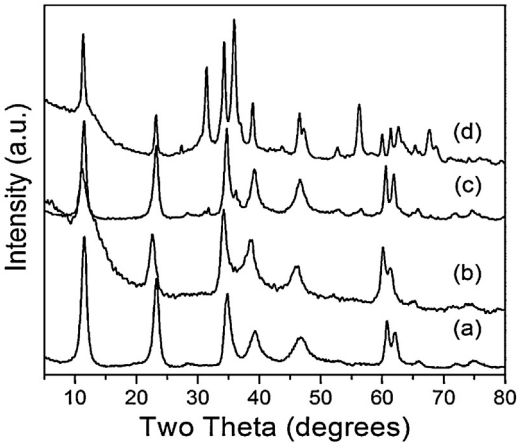

Fig. 7. XRD patterns for calcined LDHs, (a)MgAl, (b)MgZnAl-5, (c)MgZnAl-10 and (d) ZnAl after photocatalysis reaction of CrO_4^{2-} for 70 min.

phase present is the LDH phase, characterized by sharp peaks at low 2θ values, which correspond to the 0 0 l planes, and in-plane reflections at higher angles. The solids are crystallized, as inferred from the narrowness of peaks. As stated before, the reconstruction process consists not only on the rehydroxilation of the brucite-like sheets but also on structure reconstruction by CrO_4^{2-} anions intercalation. Nevertheless, the reconstruction process is not complete in any of the cases as may be appreciated in Fig. 5. The kinetics of this process may be affected by chemical composition, where a larger amount of magnesium would help the structure recover its original layered form faster, as observed by the diffraction patterns of MgAl and MgZnAl-10, where a near total reconstruction is observed. On the other hand, ZnAl still shows major peaks corresponding to ZnO, and the 0 0 3 peak corresponding to the LDH phase is barely emerging. Furthermore, the benefit for adsorption purposes of having simultaneously Zn and Mg in the calcined LDH compound has already been reported [43] and ascribed to different sorption mechanism occurring in Zn containing adsorbents than in the binary compounds (i.e. MgAl or ZnAl LDH compounds). In the former the sorption of CrO_4^{2-} anions has been suggested to occur predominantly by binding these ions to their surface while in the latter the sorption is presumed to occur mainly by intercalation in the layered structure (reaction 2) [44].

3.3. Photocatalytic tests

3.3.1. Effect of Zn content

Fig. 6 shows the effect of Zn content on the reduction of Cr(VI) fraction in solution. It can be observed that the rate of disappearance of Cr(VI) from solution is highly correlated with the zinc content in the solid. In this sense, it is worth noticing that the fastest Cr (VI) elimination (see Table 2) is provided by the LDH's with the highest (ZnAl) and minimum (MgZnAl-5) Zn content.

Table 2
Comparison of initial removal rate under photocatalysis and adsorption.

Material	$-r_{Ao}$	$-r_{Ao}$
	(mol L^{-1} s^{-1})	(mol L^{-1} s^{-1})
	Adsorption	Photocatalysis
MgAl	3.30E-08	2.47E-08
MgZnAl-5	5.93E-08	6.34E-08
MgZnAl-10	2.91E-08	3.74E-08
ZnAl	3.01E-08	5.77E-08
TiO_2	2.05E-08	2.28E-08

By comparing the initial rates of removal (see Table 2) it can be concluded that in the case of MgZnAl-5 the effect of UV radiation on Cr(VI) removal is practically negligible so that the observed results in Fig. 6 for this material is the result of mainly adsorption. An increase of the content of Zn (MgZnAl-10) also increases the Cr(VI) reduction rate by action of light (see Table 2). When employing ZnAl the effect of UV radiation is more evident and significant thus the enhancement can be ascribed to the increased amount of semiconductor and its interaction with UV light, which is expected to produce charge carriers h^+/e^- according to reaction 3. This phenomenon is mainly expected with ZnAl since its band gap is 3.3 eV (similar to TiO_2 Degussa P25). In this study e^- is considered the mean reagent to achieve Cr(VI) reduction. Nevertheless, h^+ plays an important role also since it favors water dissociation and HO• radical formation by reaction (4). These adsorbed hydroxyl radicals could be reduced by conduction-band electrons (reaction (5)) and thus promote structure reconstruction by rehydroxilation.

$$\text{Oxide} + h\nu \rightarrow \text{Oxide}(h^+_{+VB} + e^-_{CB}) \quad (3)$$

$$\text{Oxide}(h^+_{VB}) + H_2O_{ad} \rightarrow \text{Oxide} + HO^{\bullet}{}_{ad} + H^+ \quad (4)$$

$$\text{Oxide}(e^-_{CB}) + HO^{\bullet}{}_{ad} \rightarrow \text{Oxide} + HO^-_{ad} \quad (5)$$

$$CrO_4^{2-} + 4H_2O + 3e^- \rightarrow Cr(OH)_3 + 5OH^- \quad (6)$$

Hence, it can be concluded that the calcined LDH's with high content of Zn exhibit an important degree of photocatalytic activity that leads to achieve 100% removal of Cr(VI) by adsorption and reduction without the addition of further chemicals. This is worth pointing out since the photo-induced removal of Cr(VI) with other photocatalysts has been previously conducted under the imminent and compulsory addition of other chemicals in order to adjust pH [9].

3.4. Characterization of solids after photocatalytic tests

3.4.1. X-ray diffraction

Fig. 7 displays the XRD patterns of samples taken after photocatalytic experiments. A regeneration of the LDH structure is observed, which proceeds to a greater extent than in the adsorption experiments. This may be ascribed to UV light promoting the reconstruction of the hydrotalcite like structure mainly by rehydroxilation by means of reactions (3)–(6).

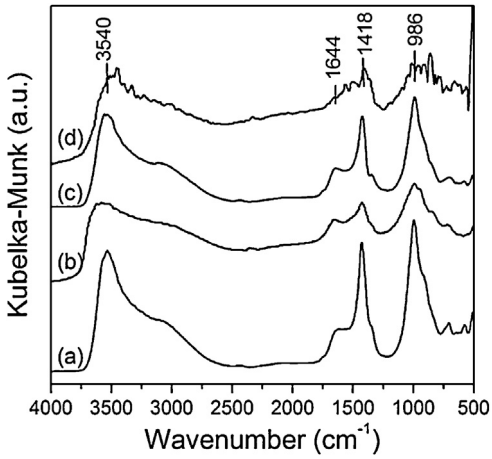

Fig. 8. FTIR spectra of samples (a)MgAl, (b) MgZnAl-5, (c) MgZnAl-10 and (d)ZnAl, taken after photocatalytic tests.

3.4.2. IR

Fig. 8 presents the FTIR spectra of samples after photocatalytic degradation of Cr(VI). A broad band is observed between *ca.* 2600 and 3800 cm^{-1}, which is ascribed to the overlapping of two or possibly even three OH stretching vibrations, and one vibration due to interlayer water [45]. There is also a vibration band at 1650 cm^{-1}, assigned to the bending vibration of water [46]. These vibration bands provide further evidence of the partial reconstruction of the original layered structure due to memory effect. Furthermore, the vibration band close to 1400 cm^{-1} is ascribed to interlayer CO_3^{2-} anions, which are trapped by the LDH either during photocatalytic tests or possibly during sample preparation, as LDHs are well known for their affinity for carbonate and easily trap it from ambient. Additionally, there is a vibration band in the low frequency region, *ca.* 980 cm^{-1}, that corresponds to an M—O vibration of lattice metals [47]. The main vibration bands for Cr (VI) are located at 940 (Cr═O) and 750 (Cr—O) cm^{-1} [48]. No vibration bands are observed around 750 cm^{-1} for any of the catalysts. Meanwhile, the band at 940 cm^{-1} could be overlapped with M—O vibrations from the LDH. Therefore, the presence of adsorbed Cr (VI) species cannot be ruled out. However, there are significant differences in initial removal rates between adsorption and photocatalysis in all Zn-containing materials. Therefore, reduction of Cr (VI) to Cr (III) must be taking place, thus displacing the equilibrium and aiding in faster and more significant removal of Cr (VI) species from solution.

4. Conclusions

Calcined MgZnAl and ZnAl hydrotalcite like compounds are versatile and possess a dual capacity that allows them to be applied for the efficient removal of Cr(VI) from solutions either by adsorption or photocatalysis. The former process is dominated by textural properties while the rate of the latter depends mainly on the Zn content, which directly affects band gap. The use of these materials as photocatalyst of anionic pollutants reduction (i.e. CrO_4^{2-}) eliminates the need of adding further chemicals reagents to adjust pH. Under the studied conditions Cr(VI) was removed by adsorption and/or photocatalysis in a range of 90–99.5% depending on Zn content and time of illumination.

Acknowledgments

CONACYT Project 153828 and PROMEP Project 103.5/09/1284 for financial support and C. Alanis acknowledges scholarship 248373 from CONACYT.

References

[1] N. Tanaka, Electrochimica Acta 21 (1976) 701–710.
[2] V. Mavrov, T. Erwe, C. Blöcher, H. Chmiel, Desalination 157 (2003) 97–104.
[3] B. Galán, D. Castañeda, I. Ortiz, Journal of Hazardous Materials 152 (2008) 795–804.
[4] L. Charerntanyarak, Water Science and Technology 39 (1999) 135–138.
[5] T.A. Kurniawan, W. Lo, G.Y. Chan, Journal of Hazardous Materials 129 (2006) 80–100.
[6] J. Yoon, G. Amy, J. Chung, J. Sohn, Y. Yoon, Chemosphere 77 (2009) 228–235.
[7] Y.C. Huang, S.S. Koseoglu, Waste Management 13 (1993) 481–501.
[8] E. Ramos-Ramírez, N.L.G. Ortega, C.A.C. Soto, M.T.O. Gutiérrez, Journal of Hazardous Materials 172 (2009) 1527–1531.
[9] S. Chakrabarti, B. Chaudhuri, S. Bhattacharjee, A.K. Ray, B.K. Dutta, Chemical Engineering Journal 153 (2009) 86–93.
[10] P. Mohapatra, S.K. Samantaray, K. Parida, Journal of Photochemistry and Photobiology A: Chemistry 170 (2005) 189–194.
[11] Y. Ku, I.-L. Jung, Water Research 35 (2001) 135–142.
[12] J. Doménech, J. Muñoz, Electrochimica Acta 32 (1987) 1383–1386.
[13] X. Liu, L. Pan, Q. Zhao, T. Lv, G. Zhu, T. Chen, T. Lu, Z. Sun, C. Sun, Chemical Engineering Journal 183 (2012) 238–243.
[14] J.S. Valente, F. Tzompantzi, J. Prince, Applied Catalysis B: Environmental 102 (2011) 276–285.
[15] E. Martín del Campo, J.S. Valente, T. Pavón, R. Romero, Á. Mantilla, R. Natividad, Industrial and Engineering Chemistry Research 50 (2011) 11544–11552.
[16] J. Zhang, F. Zhang, L. Ren, D.G. Evans, X. Duan, Materials Chemistry and Physics 85 (2004) 207–214.
[17] F. Cavani, F. Trifirò, A. Vaccari, Catalysis Today 11 (1991) 173–301.
[18] A. Vaccari, Applied Clay Science 22 (2002) 75–76.
[19] A. Guida, M.H. Lhouty, D. Tichit, F. Figueras, P. Geneste, Applied Catalysis A: General 164 (1997) 251–264.
[20] S. Albertazzi, F. Basile, A. Vaccari, Interface Science and Technology 1 (2004) 496–546.
[21] E. Álvarez-Ayuso, H.W. Nugteren, Water Research 39 (2005) 2535–2542.
[22] J.S. Valente, F. Tzompantzi, J. Prince, J.G.H. Cortez, R. Gomez, Applied Catalysis B: Environmental 90 (2009) 330–338.
[23] J.S. Valente, F. Figueras, M. Gravelle, P. Kumbhar, J. Lopez, J.P. Besse, Journal of Catalysis 189 (2000) 370–381.
[24] F. Figueras, J. Lopez, J. Sanchez-Valente, T.T.H. Vu, J.M. Clacens, J. Palomeque, Journal of Catalysis 211 (2002) 144–149.
[25] X. Jia, D. Li, D.G. Evans, Y. Lin, Particuology 8 (2010) 231–233.
[26] X. Guo, F. Zhang, Q. Peng, S. Xu, X. Lei, D.G. Evans, X. Duan, Chemical Engineering Journal 166 (2011) 81–87.
[27] E.M. Seftel, E. Popovici, M. Mertens, K.D. Witte, G.V. Tendeloo, P. Cool, E.F. Vansant, Microporous and Mesoporous Materials 113 (2008) 296–304.
[28] Á. Patzkó, R. Kun, V. Hornok, I. Dékány, T. Engelhardt, N. Schall, Colloids and Surfaces A: Physicochemical and Engineering Aspects 265 (2005) 64–72.
[29] Y. Zhao, M. Wei, J. Lu, Z.L. Wang, X. Duan, ACS Nano 3 (2009) 4009–4016.
[30] A. Mantilla, F. Tzompantzi, J.L. Fernández, J.A.I.D. Góngora, R. Gómez, Catalysis Today 150 (2010) 353–357.
[31] F. Rouquerol, J. Rouquerol, K. Sing, Adsorption by Powders and Porous Solids, Academic Press, London, 1999, pp. 219–236.
[32] Y. Li, B. Gao, T. Wu, D. Sun, X. Li, B. Wang, F. Lu, Water Research 43 (2009) 3067–3075.
[33] S.V. Prasanna, R.A.P. Rao, P.V. Kamath, Journal of Colloid and Interface Science 304 (2006) 292–299.
[34] N.K. Lazaridis, D.D. Asouhidou, Water Research 37 (2003) 2875–2882.
[35] S. Martinez-Gallegos, H. Pfeiffer, E. Lima, M. Espinosa, P. Bosch, S. Bulbulian, Microporous and Mesoporous Materials 94 (2006) 234–242.
[36] K.-H. Goh, T.-T. Lim, Z. Dong, Water Research 42 (2008) 1343–1368.
[37] R.L. Goswamee, P. Sengupta, K.G. Bhattacharyya, D.K. Dutta, Applied Clay Science 13 (1998) 21–34.
[38] M.J. Holgado, F.M. Labajos, M.J.S. Montero, V. Rives, Materials Research Bulletin 38 (2003) 1879–1891.
[39] C.H. Weng, J.H. Wang, C.P. Huang, Water Science and Technology 35 (1997) 55–62.
[40] J.C. Yu, X.-J. Wu, Z. Chen, Analytica Chimica Acta 436 (2001) 59–67.
[41] N.F. Fahim, B.N. Barsoum, A.E. Eid, M.S. Khalil, Journal of Hazardous Materials 136 (2006) 303–309.
[42] S. Martínez-Gallegos, V. Martínez, Separation Science and Technology 39 (2004) 667–687.
[43] J.S. Valente, H. Pfeiffer, E. Lima, J. Prince, J. Flores, Journal of Catalysis 279 (2011) 196–204.
[44] B. Dudek, P. Kuśtrowski, A. Białas, P. Natkański, Z. Piwowarska, L. Chmielarz, M. Kozak, M. Michalik, Materials Chemistry and Physics 132 (2012) 929–936.
[45] V. Rives, Layered Double Hydroxides: Present and Future, first ed., Nova Science Publishers, New York, 2001.
[46] K. Nakamoto, Infrared and Raman Spectra of Inorganic and Coordination Compounds, fifth ed., John Wiley & Sons, New York, 1997.
[47] A. Legrouri, M. Lakraimi, A. Barroug, A. De Roy, J.P. Besse, Water Research 39 (2005) 3441–3448.
[48] J.G. Ko, U.S. Choi, T.Y. Kim, D.J. Ahn, Y.J. Chun, Macromolecular Rapid Communications 23 (2002) 535–539.